

## Methodological Issues in Lipid Bilayer Simulations

Céline Anézo,<sup>†</sup> Alex H. de Vries,<sup>‡</sup> Hans-Dieter Höltje,<sup>†</sup> D. Peter Tieleman,<sup>§</sup> and Siewert-Jan Marrink<sup>\*,‡</sup>

*Institute of Pharmaceutical Chemistry, University of Düsseldorf, Universitätsstr. 1, D-40225 Düsseldorf, Germany, Department of Biophysical Chemistry, University of Groningen, Nijenborgh 4, 9747 AG Groningen, The Netherlands, and Department of Biological Sciences, University of Calgary, 2500 University Drive NW, Calgary, Alberta T2N 1N4, Canada*

*Received: April 5, 2003; In Final Form: June 12, 2003*

Methodological issues in molecular dynamics (MD) simulations, such as the treatment of long-range electrostatic interactions or the type of pressure coupling, have important consequences for the equilibrium properties observed. We report a series of long (up to 150 ns) MD simulations of dipalmitoylphosphatidylcholine (DPPC) bilayers in which the methodology of simulation is systematically varied. Comparisons of simulations with truncation schemes, Ewald summations, and modified Coulomb interactions, either by shift functions or reaction field models, to describe long-range electrostatics point out the artifacts inherent in each of these methods and above all those of straight cutoff methods. We further show that bilayer properties are less sensitive to the details of the pressure-coupling algorithm and that an increased integration time step of 5 fs can be safely used in simulations of phosphatidylcholine lipid bilayers.

### I. Introduction

Phospholipid bilayers represent the fundamental structure of most biomembranes. In the biologically relevant liquid-crystal-line state, these lipid assemblies exhibit very complex structural and dynamic properties due to an extreme fluidity accompanied by an inherent disorder. Motions with a range of time constants are present in lipid bilayers, making their theoretical study particularly challenging. Whereas individual motions such as conformational changes occur on a time scale of tens to hundreds of picoseconds, the complete rotation of a phospholipid molecule around its long axis requires a few nanoseconds, and tens of nanoseconds are needed to observe lateral diffusion. Events such as the flip-flop of a lipid molecule from one leaflet to the opposite one even take place on a typical time scale of minutes to hours.<sup>1</sup>

Molecular dynamics simulations constitute an irreplaceable tool for the visualization of such phenomena and offer insightful pictures of membrane structure and dynamics. MD simulations are primarily limited by the system size, accessible time scale, and accuracy of the force field that describes the interactions in the system. Currently, simulations typically involve a few hundred of lipids and are confined to a few nanoseconds.<sup>2–5</sup> Recently, Lindahl and Edholm<sup>6,7</sup> reported the first 100-ns simulation of a bilayer consisting of 64 DPPC molecules, and a larger system containing 1024 lipids with a linear size of 20 nm was simulated for 10 ns. Marrink and Mark<sup>8</sup> carried out a series of monoolein (MO) bilayer simulations, reaching system sizes up to 20 nm and time scales up to 40 ns. This time scale order is required to follow the lateral diffusion of individual lipids adequately, whereas the simulation of large patches allows one to discern collective phenomena such as undulation motions.

One of the most frequently used techniques in biomolecular simulations to speed up the computations is the truncation of the long-range electrostatic forces. These so-called cutoff methods are also widely used in membrane simulations, including some of the studies mentioned above. However, such approximations belong to the most drastic ones in a simulation procedure and can therefore have a significant influence on the system properties. To circumvent the abrupt truncation of the electrostatic interactions, “shift” or “switch” functions can be applied to smooth the interaction energy or force to zero either within the whole cutoff range or over a limited region. Two widespread alternative methods that include the effect of long-range electrostatic interactions are the particle mesh Ewald (PME) and moving-boundary reaction field (RF) approaches. PME<sup>9,10</sup> is based on an interpolation of the reciprocal-space Ewald sum. The central simulation cell is replicated by the periodic boundary conditions, and all of the electrostatic interactions in this periodically replicated system are summed. PME is a well-established method for the rigorous treatment of long-range electrostatics in periodic systems.<sup>11,12</sup> In the RF approach,<sup>13</sup> the electrostatic interactions are corrected for the effect of the polarizable surroundings beyond the cutoff radius. This method has been developed for homogeneous systems, for instance, for liquid simulations, or for a small solute immersed in a solvent. Within the cutoff sphere, solute and solvent are simulated in atomic detail, whereas the solvent outside the sphere is treated as a dielectric continuum.

A number of studies compare the methods of treating long-range electrostatics. In bulk water, for instance, several studies<sup>12,14–16</sup> show an artificial ordering of water when using a Coulomb cutoff method, resulting in a higher viscosity. The artifacts induced by the Coulomb cutoff are particularly clear in the analysis of the water dipole correlations: the water dipoles are anticorrelated slightly below the cutoff and correlated slightly above the cutoff. A significant decrease of the long-range dipole correlation is observed with the RF approach and especially

\* Corresponding author. E-mail: marrink@chem.rug.nl. Fax: +31-50-3634800.

<sup>†</sup> University of Düsseldorf.

<sup>‡</sup> University of Groningen.

<sup>§</sup> University of Calgary.

with PME. However, short- and intermediate-range correlations are still stronger with RF than with PME. The use of electrostatic cutoffs has similar effects on the water structure in interfacial systems, including the water/lipid interface.<sup>14,17</sup> Furthermore, cutoff-induced ordering strongly affects the structure of ionic solutions.<sup>13,18</sup>

The Ewald technique may induce artificial effects due to the infinite periodicity implied by this technique. The Ewald-enhanced stability of peptides, for instance, has been observed in a number of simulations.<sup>19–21</sup> Periodicity artifacts were found to be particularly important in systems involving a solvent of low dielectric permittivity, a small unit cell, or a solute with a net charge or a large dipole. Venable and co-workers<sup>22</sup> carried out a series of MD simulations of a DPPC bilayer in the gel state, applying the Ewald summation and spherical cutoff methods. Better agreement with experiment was found for the lamellar spacing and the chain tilt in simulations using the Ewald summation, and the molecular area was better reproduced by spherical cutoff methods. Simulation times were between 0.2 and 2.5 ns, which might not be sufficient for conclusions to be drawn about these methods. Instead of 3D Ewald summation methods, one can also use 2D versions that contain correction terms for slab geometries.<sup>23,24</sup> These methods are shown to be faster and more accurate than previous versions of 2D Ewald yet not as fast as 3D methods. A pseudo-2D system can be generated by including a large vacuum layer separating the slab from its periodic image. Recent simulations of a water channel inside a lipid bilayer show that the ordering of water inside the channel is strongly enhanced when using 3D Ewald compared to the pseudo-2D method.<sup>25</sup> Erroneous results using 3D Ewald for interfacial systems were also reported by Yeh and Berkowitz.<sup>23</sup> Tieleman et al.<sup>26</sup> simulated alamethicin channels embedded in a lipid bilayer, comparing the effects of twin-range cutoff, PME, and RF methods on the water orientation inside the channels. The ordering degree of water within the pore was found to be significantly lower in PME and RF simulations than in cutoff simulations. The water orientation was, however, better reproduced with the PME than with the RF approach, making the Ewald treatment the method of choice for this system and thus suggesting that the periodicity artifacts are minor.

A priori, none of the electrostatic methods mentioned above seem to be very well suited for membrane simulations. The cutoff method induces artificial ordering, the PME method enhances periodicity, and the RF method ignores the heterogeneous nature of the membrane.

The effect of the choice of handling the long-range electrostatic interactions on membrane properties has never been systematically investigated in long-time simulations. We attempt to do so in the present study. An extensive series of simulations was carried out of a fully hydrated DPPC bilayer in the biologically relevant liquid-crystalline state. We compare four methods for the treatment of electrostatics: a standard group-based truncation method, the PME summation method, the RF method, and the use of shift functions. The size of cutoff radii was tested in the truncation, reaction field, and shift function methods. We also experimented with different groupings of the partial charges in the phospholipids.

The choice of macroscopic boundary conditions<sup>27,28</sup> and pressure-coupling algorithms can significantly influence the system characteristics as well. Therefore we also tested different pressure-coupling types and algorithms. Finally, the effect of an increased integration time step was evaluated. The present work does not aim at testing force fields but concentrates exclusively on methodology. To reduce the possibility that the

observed effects are linked to the chosen system setup, however, systems were simulated using two different force fields and at two different sizes. The amount of hydration water was also varied.

An accurate comparison of simulation procedures requires long simulation times to be able to distinguish differences in equilibrium quantities unambiguously; sampling times that are too short often lead to erroneous conclusions. The simulation time was thus extended up to 150 ns in some cases to cover a broad spectrum of modes of motion. Special attention was devoted to the response of the membrane area to the simulation conditions. This structural quantity not only describes the molecular packing of the bilayer but also provides information on the degree of membrane fluidity. The area per lipid is very sensitive to simulation details and is generally considered to be a reliable criterion for comparing and validating calculations.

## II. Methods

**A. Simulated Systems.** In the first series of simulations (A–F), the membrane system consists of 128 DPPC molecules surrounded by 3726 water molecules, corresponding to 29 waters per lipid and to a fully hydrated state<sup>29</sup> of the bilayer. Two additional simulations (G and H) were carried out at a lower degree of hydration at a water-to-lipid ratio of 6, reducing the total number of water molecules to 776. The second series of simulations (I–L) was performed on a membrane system consisting of 256 DPPC molecules surrounded by 8896 water molecules, corresponding to 35 waters per lipid.

**B. Force Fields.** The force fields used in this study are variations on the united-atom DPPC force field described by Berger et al.,<sup>30</sup> who parametrized the Lennard-Jones (LJ) parameters for the hydrocarbon tails using a cutoff of 1.0 nm for the LJ interactions and an isotropic long-range dispersion correction. The first set of simulations (A–H) was performed using this force field without applying the long-range dispersion correction, except for simulation B2b. Recently, a new set of hydrocarbon parameters that reproduced new vaporization data<sup>31</sup> and was parametrized for a LJ cutoff of 1.4 nm without the use of a long-range dispersion correction<sup>32</sup> became available. These parameters were used in the second series of simulations (I–L). The new parameters, however, make the tails more attractive, and applying these to phospholipid bilayers led to gel-phase structures. The balance between lipid tail attraction and lipid headgroup repulsion was restored by enhancing headgroup hydration by making the LJ interactions between lipid atoms and the water oxygen atom more attractive. The parameters used for the water oxygen in the interaction with lipid atoms were  $\sigma = 0.3113$  nm and  $\epsilon = 0.7184$  kJ/mol. Also, the ester and phosphate doubly bound O atoms were given different LJ parameters to enhance the hydration of the headgroup. The parameters used for C=O and P=O were  $\sigma = 0.296$  nm and  $\epsilon = 0.810$  kJ/mol. By using these two different force fields, the dependence of the electrostatic treatment effects on the balance between attractive and repulsive forces in the bilayer may be assessed.

In both series, partial charges were taken from ab initio electronic structure computations,<sup>33</sup> and 1,4 electrostatic interactions were scaled by a factor of 2. 1,4 Lennard-Jones interactions were scaled by a factor of 8. For water, the simple point-charge (SPC) model<sup>34</sup> was chosen.

**C. Electrostatics.** Several electrostatics treatments were applied for both force fields. A twin-range cutoff scheme was employed in simulations A, B1–3, C, G, and I1–3. In simulations A, B1–3, C, and G, short-range electrostatic

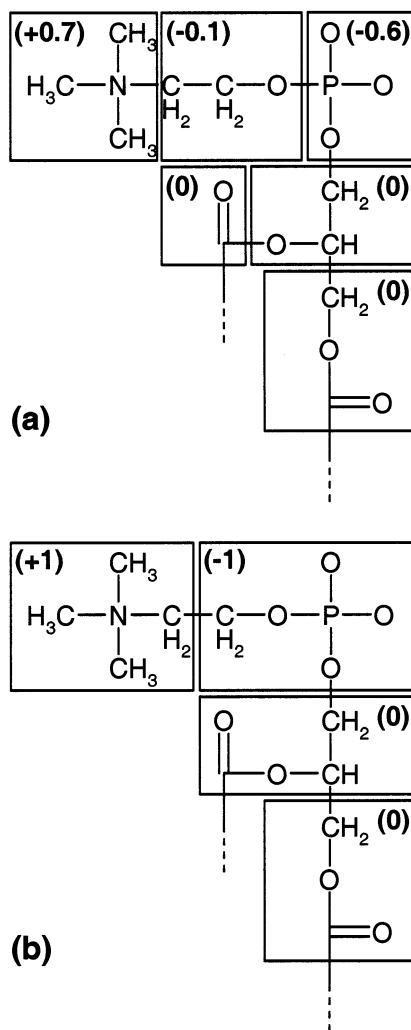


**Figure 1.** Charge-group definition in the DPPC headgroup part, with the net charge per group indicated in parentheses. (a) Six charge groups. (b) Four charge groups.

interactions were calculated for every time step within a sphere of 1-nm radius, whereas long-range electrostatic interactions were calculated within the long-range cutoff sphere only every 20 fs and then kept constant until the next update. The standard long-range electrostatic cutoff,  $R_C$ , was 1.8 nm (A, B1, C, and G). Two additional values for  $R_C$  were tested—a smaller one of 1.4 nm (B2a) and a larger one of 2.4 nm (B3)—to observe any influence on the membrane behavior. In simulations I1–3, the short-range cutoff was 1.4 nm, and  $R_C$  was varied from 1.5 nm (I1) to 2.0 nm (I2) to 3.0 nm (I3). The spherical truncation technique selected here is based on charge groups: neighboring atoms are gathered together to form relatively small groups, ideally with no net charge. A neighbor list includes all atom pairs belonging to charge groups within the cutoff radius for which nonbonded interactions are calculated. This group-based method enables one to avoid the creation of artificial charges cutting through dipoles. Ideally, charge groups should be both small and electrically neutral. In the case of the DPPC headgroup, this is not possible. To test the influence of the definition of the charge groups, we simulated two different charge-group distributions. One consists of six small groups possessing net charges as small as possible (Figure 1a), whereas the other defines four large groups with integer charges (Figure 1b). The latter was tested in simulations A and D; all other simulations use the distribution with six small groups.

The PME method was tested in simulations D, E1–3, H, and J. In simulations D, E1–3, and H, a cutoff of 1 nm was applied in the direct-space sum for short-range interactions. For the calculation of long-range interactions in reciprocal space, the charges were projected onto a grid using cubic interpolation. This grid was then Fourier transformed with a 3D FFT (fast Fourier transform) algorithm using a maximum spacing of 1.2 Å for the FFT grid. In simulation J, the direct-space sum cutoff was 1.4 nm.

Moving-boundary reaction field conditions were tested in simulations F and K1–3. A relative dielectric constant of 1 was applied within the spherical cutoff region, and the region beyond the cutoff was assumed to have a dielectric constant of 80, corresponding to the experimental value for water. Tironi et al.<sup>13</sup> simulated their system consisting of sodium and chloride ions immersed in SPC water molecules with a dielectric constant of 80, and Hünenberger and van Gunsteren,<sup>15</sup> in pure SPC water simulations, set the dielectric constant to 54, corresponding to the self-consistent value reported for SPC water.<sup>35</sup> We tested both values (simulations not shown) and did not observe any effect on the membrane properties. In simulation F, a cutoff of 1.8 nm was adopted. In simulations K1–3, the cutoff distance was varied from 1.4 to 3.0 nm to assess the sensitivity of the approach to the electrostatic cutoff.

Finally, the effect of a shift function<sup>36</sup> was tested (L1,2). Coulomb interactions were modified so that both energy and force vanish at the cutoff distance, using a smooth shift function from 0.0 nm to the cutoff distance. The long-range cutoff was varied between 1.4 nm (L1) and 2.0 nm (L2). In both runs, the Lennard-Jones interactions were also altered to vanish at the short-range cutoff distance of 1.4 nm, using a switch function, starting the modification of the interaction energy and force at 1.0 nm.

**D. Macroscopic Boundary Conditions and Pressure Coupling.** All simulations were done under constant pressure conditions so that the size and the shape of the simulation box were free to adjust, allowing the membrane area and thickness to fluctuate. This offers the possibility to compare and validate simulations by examining their ability to reproduce important structural quantities such as the projected area per lipid. The correct ensemble for this system would be  $N\gamma p_N T$ , in which the surface tension and the normal pressure are specified.<sup>37</sup> The surface tension is defined by:

$$\gamma = \int_{-\infty}^{\infty} (p_N - p_L(z)) dz$$

$p_N$  is the pressure in the direction normal to the bilayer, and  $p_L$  is the lateral pressure. In the simulations, the pressure was controlled either anisotropically or semi-isotropically. In the former case, the three unit-cell dimensions fluctuate independently from each other, and the total pressure  $P$  remains constant. This corresponds to an  $Np_x p_y p_z T$  ensemble, which is not rigorously defined and stable only when at least two of the pressure components are equal. The semi-isotropic case corresponds to  $Np_N p_L T$ . In both cases, the pressure components are kept at 1 bar on average. The only difference in the simulations is that in the anisotropic case the simulation box fluctuates independently in  $x$  and  $y$  whereas in the semi-isotropic case the interface maintains a square. When the lateral pressure and normal pressure are equal, the average surface tension is zero; at constant box length, specifying zero surface tension and a normal pressure of 1 bar is equivalent to specifying a lateral and normal pressure of 1 bar. We ignore the effect of the fluctuating box length and assume that specifying a lateral and



TABLE 1: Overview of MD Simulations

label <sup>a</sup>	electrostatics <sup>b</sup>	charge groups	pressure coupling		$n_w$ <sup>c</sup>	simulation time (ns)	time step (fs)	speed <sup>d</sup> (h/ns)
			algorithm	type				
A	cutoff (1.8 nm)	4	Berendsen	anisotropic	29	150	5	20
B1	cutoff (1.8 nm)	6	Berendsen	anisotropic	29	150	5	20
B2a	cutoff (1.4 nm)	6	Berendsen	anisotropic	29	150	5	15
B2b <sup>e</sup>	cutoff (1.4 nm)	6	Berendsen	anisotropic	29	100	5	15
B3	cutoff (2.4 nm)	6	Berendsen	anisotropic	29	150	5	35
C	cutoff (1.8 nm)	6	Berendsen	anisotropic	29	50	2	30
D	PME	4	Berendsen	anisotropic	29	150	5	20
E1	PME	6	Berendsen	anisotropic	29	150	5	20
E2	PME	6	Parrinello	anisotropic	29	150	5	20
E3	PME	6	Berendsen	semiisotropic	29	150	5	20
F	RF (1.8 nm)	6	Berendsen	anisotropic	29	150	5	20
G	cutoff (1.8 nm)	6	Berendsen	anisotropic	6	150	5	10
H	PME	6	Berendsen	anisotropic	6	150	5	10
I1	cutoff (1.5 nm)	6	Berendsen	anisotropic	35	40	5	55
I2	cutoff (2.0 nm)	6	Berendsen	anisotropic	35	30	5	65
I3	cutoff (3.0 nm)	6	Berendsen	anisotropic	35	20	5	95
J	PME	6	Berendsen	anisotropic	35	35	5	85
K1	RF (1.4 nm)	6	Berendsen	anisotropic	35	35	5	60
K2	RF (2.0 nm)	6	Berendsen	anisotropic	35	40	5	70
K3	RF (3.0 nm)	6	Berendsen	anisotropic	35	35	5	105
L1 <sup>f</sup>	shift (1.4 nm)	6	Berendsen	anisotropic	35	40	5	80
L2 <sup>f</sup>	shift (2.0 nm)	6	Berendsen	anisotropic	35	17	5	90

<sup>a</sup> In the first series of simulations (from A to H), the system consists of 128 DPPC molecules. In the second series (from I to L), the system contains 256 DPPC molecules. In the first and second series, LJ cutoffs of 1.0 and 1.4 nm are used, respectively. The two series use a different force field. <sup>b</sup> The long-range Coulomb cutoff is given in parentheses. <sup>c</sup>  $n_w$  corresponds to the number of water molecules per DPPC molecule. <sup>d</sup> The simulation rate is that reached with the GROMACS package, versions 2.1 and 3.0, on a dual-processor Pentium PIII 1-GHz node. <sup>e</sup> A long-range dispersion correction is applied in simulation B2b. <sup>f</sup> The LJ interactions were smoothly switched to zero from 1.0 to 1.4 nm.

normal pressure of 1 bar is the same as specifying zero surface tension and a normal pressure of 1 bar.<sup>37</sup>

A weak pressure-coupling scheme<sup>38</sup> was adopted in most of the simulations. Because the Berendsen algorithm does not produce a perfect *NPT* ensemble, the Parrinello–Rahman barostat<sup>39</sup> was also tested in simulation E2. This algorithm better reproduces pressure fluctuations and may also affect equilibrium properties such as the membrane area.

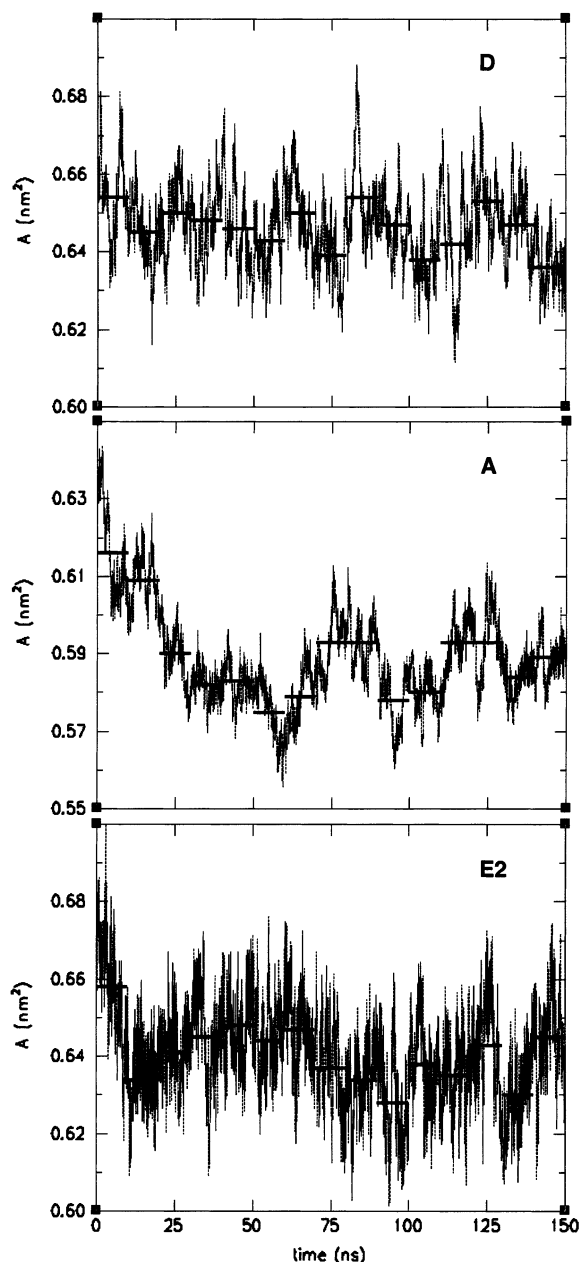
**E. Simulation Conditions.** All simulations were performed with the molecular dynamics package GROMACS,<sup>40</sup> versions 2.1 and 3.0. (Both versions give the same results.) Timings are reported for dual-processor Pentium PIII 1-GHz nodes. Periodic boundary conditions were applied in all three dimensions so that actually a multilamellar system is simulated. Simulations were carried out at a constant pressure of 1 bar and a constant temperature of 323 K. DPPC and water were coupled independently to the heat bath. The coupling times for temperature and pressure were set at 0.1 and 1 ps, respectively. All bond lengths in DPPC were kept constant using the LINCS routine,<sup>41</sup> and the water geometry was maintained with the SETTLE algorithm.<sup>42</sup> The efficiency and stability of both algorithms allow a time step of 5 fs.<sup>43</sup> Owing to this relatively large time step, simulation times could be extended up to 150 ns. One system was simulated for 50 additional nanoseconds with a time step of 2 fs (simulation C) without any change in the equilibrium properties, demonstrating that a time step of 5 fs provides enough accuracy.

Table 1 gives a summary of the calculations performed.

### III. Results

**A. Equilibration and Fluctuations of Structural Properties.** Depending on the simulation, the instantaneous projected area per lipid shows rather slow convergence. Figure 2 displays the time evolution of the area per DPPC for three selected simulations. In simulation D, the equilibration of the area requires only a couple of nanoseconds, but in simulation A,

the area continues to decrease until 25 ns of simulation time has been reached. Simulation E2 represents an intermediate case, where convergence is reached after 10 ns. The time needed for equilibration does not appear to depend strongly on the method used, however, but rather on the difference between the initial and final area per lipid. This is not always true; sometimes equilibration is reached after a few nanoseconds, although the difference between the initial and final area per lipid is considerable. Because of this slow relaxation, data were analyzed starting at 25 ns for simulations A–H. In simulations I–L, relaxation was usually faster, and analysis was started at 10 ns. Large thermal fluctuations of the lipid area around its average value are observed after equilibrium has been reached. Table 2 gives the average area *A* per DPPC obtained for each simulation, with the standard error (SE) and correlation time ( $\tau_A$ ). An estimate of the error in the calculated area per lipid was obtained using a block average procedure. Data were divided into *n* blocks, over which subaverages were calculated. The block averages are considered to be independent of the number of blocks when the block length is much longer than the correlation time. By dividing the standard deviation of these block averages by  $n^{1/2}$ , a standard error estimate can be calculated. The function of the standard error estimates as a function of block size is then fitted to a single-exponential function. The best estimate of the standard error of the data is then given by the limit at large block size of the fitted curve. The correlation time is also obtained from this fit.<sup>12</sup> Correlation times from 1 to 10 ns have been found. However, even slower motions exist. A discrete Fourier transform analysis performed on the first series of simulations indicates two main periods in the range of 15–20 ns and 30–40 ns. A visual inspection of Figure 2 also shows the presence of such modes, independently on the simulation conditions. Even 100-ns simulation times are not sufficient to sample these modes statistically. In contrast to the area, the volume *V* per lipid converges very fast—within a few hundred picoseconds—after which it fluctuates around 1.2



**Figure 2.** Time evolution of the area per lipid in simulations D, A, and E2. The horizontal bars represent subaverages calculated over blocks of 10 ns each.

$\text{nm}^3$  with small amplitudes. The bilayer repeat distance  $L_z$ , like the area, exhibits large fluctuations. Both fluctuations are anticorrelated because the volume remains approximately constant. Average values for the volume and the lamellar repeat spacing are also listed in Table 2.

**B. Area per Lipid.** Of all of the different simulation conditions tested, the treatment of electrostatics has the largest impact on the area. In the first series, differences are especially found when applying the particle mesh Ewald summation instead of a simple cutoff (runs D and E versus A and B). Lipid areas obtained with PME are significantly higher than those obtained with an abrupt truncation of the electrostatic interactions. Taking the best standard error estimates as the standard error of an infinitely large sample, a difference in reported areas of  $0.006 \text{ nm}^2$  (or 1%) is considered to be significant. In a two-tailed student's *t*-test, such a difference corresponds to a significance level of 0.05 when taking the standard errors in

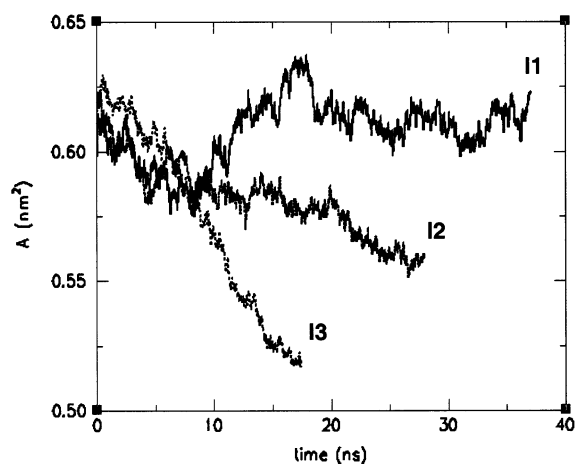
both area means as  $0.002 \text{ nm}^2$ . We performed two additional simulations (G and H) at reduced water content, corresponding to six water molecules per DPPC, to investigate whether this increase in the area depends on the hydration level. At low hydration, the area increases by 3% from cutoff to PME, demonstrating that the response of the area to PME is not related to the amount of water but rather is governed by a different balance of forces in the lipid assembly itself. In the second series, the use of PME also enlarges the area with respect to the cutoff method (J vs I). The difference between the truncation method and PME becomes larger as the cutoff radius increases. We used three values of 1.4, 1.8, and 2.4 nm for the Coulomb cutoff in the first series (B1–3). The smallest cutoff leads to the largest average area. The area drops by about 4% from  $R_C = 1.4$  (B2a) to  $R_C = 1.8$  nm (B1) and by about 2.5% from  $R_C = 1.8$  (B1) to  $R_C = 2.4$  nm (B3), which demonstrates the sensitivity of the area to the choice of the truncation radius. In the second series (I1–3), an even more dramatic contraction of the system is observed as the cutoff is increased. The total volume, volume per lipid, and (especially) area per lipid decrease as the cutoff is increased. With the force field used in the second series, it is questionable whether the system remains in the liquid-crystalline state with cutoffs of 2.0 and 3.0 nm because the area per lipid was still decreasing when the simulations were stopped. The evolution of the area per lipid is shown for the different cutoff radii in Figure 3. Note that the three systems behave similarly during the first 10 ns of simulation.

Figure 4 shows a comparison between straight cutoff, PME, and reaction field approaches for the first series. The order of the area per lipid as a function of electrostatic treatment is straight cutoff < PME < RF. The difference in the area is less between PME and RF than between PME and cutoff. In the second series, the same order is observed, although larger areas are obtained with the RF approach. Increasing the cutoff within the RF method has relatively little effect on the area per lipid compared to that obtained from the straight cutoff technique. Where a straight cutoff of 2.0 nm already led to a very small area per lipid with the second force field (I2), applying the reaction field correction with the same cutoff (K2) only moderately condenses the system compared to the RF result with the smaller cutoff of 1.4 nm (K1). Apparently, the removal of the artificial favorable interactions just inside the cutoff sphere by the reaction field method results in a system that is reasonably insensitive to the size of the cutoff sphere. In this context, the results of using a shift function, which also avoids unrealistic favorable interactions just inside the cutoff sphere but does not contain an energy term that stabilizes the dipole inside the cutoff sphere (runs L1,2), are interesting. The use of a shift function does not have as dramatic an influence on the area per lipid as does the use of the reaction field method. The area per lipid is similar to the ones seen with the smallest Coulomb cutoff (I1) and with PME (J). Increasing the cutoff radius from 1.4 to 2.0 nm with the shift function appears to increase the area per lipid, an effect opposite to that seen with the reaction field method and the straight cutoff approach. Unfortunately, the run with the larger cutoff sphere (L2) proved to be quite unstable and therefore limited in simulation time. The reason for this instability is not clear.

The size of the charge groups has a significant effect on the area. The change from larger to smaller charge groups results in an increase of the area per lipid by 2% with a Coulomb cutoff (A vs B1) and in a decrease by 2% with PME (D vs E1). The effect seen with PME can be attributed to the effect of changing

TABLE 2: Equilibrium Properties

label	$V \pm \text{SE}$ (nm <sup>3</sup> )	$L_c \pm \text{SE}$ (nm)	$A \pm \text{SE}$ (nm <sup>2</sup> )	$\text{SD}_A$ (nm <sup>2</sup> )	$\tau_A$ (ns)	$K_A \pm \text{SE}$ (mN/m)
A	1.2225 $\pm$ 0.0005	7.28 $\pm$ 0.03	0.585 $\pm$ 0.002	0.009	3.0	500 $\pm$ 100
B1	1.2204 $\pm$ 0.0005	7.14 $\pm$ 0.03	0.597 $\pm$ 0.003	0.011	5.0	350 $\pm$ 100
B2a	1.2225 $\pm$ 0.0006	6.87 $\pm$ 0.02	0.621 $\pm$ 0.002	0.010	2.0	450 $\pm$ 100
B2b	1.1717 $\pm$ 0.0004	6.79 $\pm$ 0.02	0.610 $\pm$ 0.002	0.011	1.5	350 $\pm$ 100
B3	1.2199 $\pm$ 0.0010	7.31 $\pm$ 0.06	0.583 $\pm$ 0.005	0.014	10.0	200 $\pm$ 50
C	1.2245 $\pm$ 0.0005	7.12 $\pm$ 0.03	0.599 $\pm$ 0.003	0.009	2.5	500 $\pm$ 100
D	1.2208 $\pm$ 0.0005	6.63 $\pm$ 0.02	0.646 $\pm$ 0.002	0.011	1.0	400 $\pm$ 100
E1	1.2190 $\pm$ 0.0005	6.74 $\pm$ 0.02	0.635 $\pm$ 0.002	0.010	1.5	450 $\pm$ 100
E2	1.2200 $\pm$ 0.0006	6.69 $\pm$ 0.02	0.640 $\pm$ 0.002	0.013	1.5	250 $\pm$ 50
E3	1.2200 $\pm$ 0.0005	6.71 $\pm$ 0.01	0.638 $\pm$ 0.001	0.010	1.0	450 $\pm$ 100
F	1.2180 $\pm$ 0.0004	6.62 $\pm$ 0.02	0.647 $\pm$ 0.002	0.011	3.0	400 $\pm$ 100
G	1.2200 $\pm$ 0.0006	4.85 $\pm$ 0.03	0.582 $\pm$ 0.003	0.010	7.0	400 $\pm$ 100
H	1.2221 $\pm$ 0.0004	4.72 $\pm$ 0.01	0.599 $\pm$ 0.001	0.007	2.0	850 $\pm$ 200
I1	1.2018 $\pm$ 0.0002	7.40 $\pm$ 0.03	0.613 $\pm$ 0.003	0.008	2.0	300 $\pm$ 50
I2	<1.19		<0.56			
I3	<1.18		<0.52			
J	1.1954 $\pm$ 0.0004	7.30 $\pm$ 0.03	0.623 $\pm$ 0.003	0.007	1.5	300 $\pm$ 50
K1	1.2163 $\pm$ 0.0002	6.48 $\pm$ 0.02	0.705 $\pm$ 0.002	0.008	1.0	400 $\pm$ 100
K2	1.2131 $\pm$ 0.0002	6.60 $\pm$ 0.02	0.691 $\pm$ 0.002	0.008	1.0	350 $\pm$ 100
K3	1.2111 $\pm$ 0.0002	6.72 $\pm$ 0.01	0.678 $\pm$ 0.001	0.006	0.5	600 $\pm$ 100
L1	1.2030 $\pm$ 0.0002	7.40 $\pm$ 0.04	0.614 $\pm$ 0.003	0.009	2.0	300 $\pm$ 50
L2	1.2081 $\pm$ 0.0003	7.29 $\pm$ 0.02	0.624 $\pm$ 0.002	0.006	0.5	600 $\pm$ 100
experiments <sup>a</sup>	1.232	6.7	0.633 <sup>44</sup> /0.64			231 $\pm$ 20

<sup>a</sup> See ref 45.

**Figure 3.** Time evolution of the area per lipid in simulations using different cutoff radii. The solid-line curve corresponds to run I1 ( $R_C = 1.5$  nm), the dotted-line curve, to run I2 ( $R_C = 2.0$  nm), and the dashed-line curve, to run I3 ( $R_C = 3.0$  nm).

the effective cutoff for the Lennard-Jones interactions because the electrostatic cutoff in PME serves only as a numerical device to separate direct- and reciprocal-space sums.

The introduction of a correction term into the Lennard-Jones potential to account for the long-range dispersion forces (B2b vs B2a) leads to a global compression of the bilayer system: a decrease of 2% in the area per lipid is observed, and a decrease of 4% in the volume per lipid is registered.

The effect of pressure coupling on the area per lipid is deduced from a comparison of simulations E1–3. In the case of the smaller system (first series of simulations), the anisotropic pressure coupling tends to generate a net deformation of the unit cell in the membrane plane. This anisotropy tends to be more pronounced in the PME than in the cutoff or RF runs. A simulation with semi-isotropic pressure coupling (E3) was added to avoid this large anisotropy in box sizes and to make sure that it does not alter structural membrane properties. Simulations E1 and E3, differing by the type of pressure coupling, lead to statistically indistinguishable average lipid areas. The type of

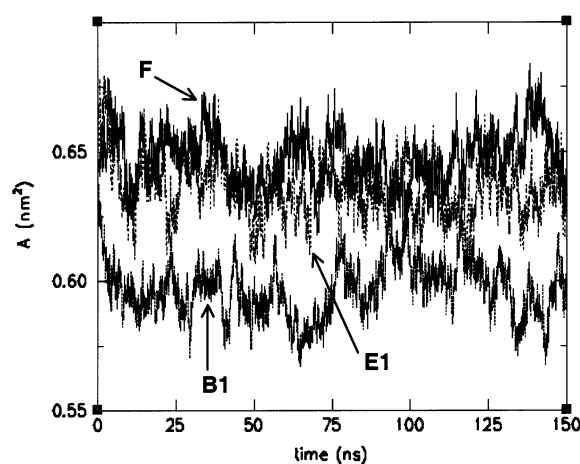


**Figure 4.** Time evolution of the area per lipid in simulations with either a Coulomb cutoff, PME, or a reaction field. The dotted-line curve corresponds to run B1, the dashed-line curve, to run E1, and the solid-line curve, to run F.

barostat used (Berendsen or Parrinello–Rahman) did not affect the equilibrium properties significantly. (Compare runs E1 and E2.)

**C. Area Compressibility.** The area compressibility modulus  $K_A$  describes an elastic property of the membrane and can be related to the variance of the lipid area  $\sigma_A^2$ :

$$K_A = \frac{k_B T A}{N \sigma_A^2}$$

$A$  denotes the average area per lipid,  $N$  is the number of lipid molecules in one layer,  $T$  is the temperature, and  $k_B$  is the Boltzmann constant. Area compressibility moduli have been calculated for all of the simulations and are listed in Table 2, together with the standard deviations ( $\text{SD}_A$ ) in the lipid areas. At full hydration of the membrane, they range from 200 to 600 mN/m and are above the experimental value of  $231 \pm 20$  mN/m.<sup>45</sup> This is due to the suppression of undulatory modes in a system of limited size.<sup>8</sup> There appears to be no direct relation

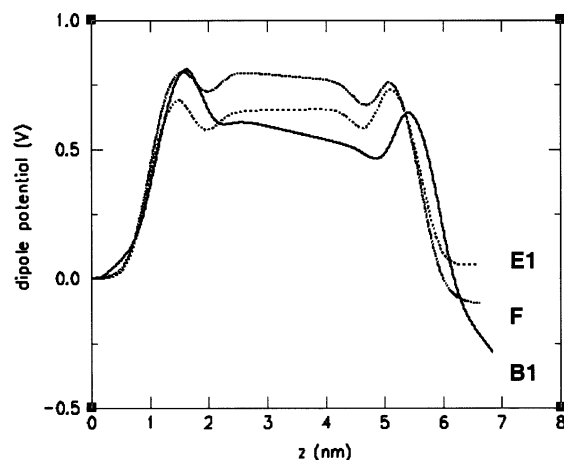


**Figure 5.** Dipole potential across the DPPC bilayer in simulations using either a Coulomb cutoff of 1.8 nm (B1, solid-line curve), PME (E1, dashed-line curve), or RF (F, dotted-line curve). The position  $z = 0$  is taken as the zero of the potential.

between the average areas and the calculated compressibility moduli. A looser membrane packing, characterized by a larger area per lipid, does not systematically lead to a lower compressibility modulus, as would be expected because of the greater flexibility of membranes with larger surface areas. However, given the large standard errors, the observed differences are not highly significant. In particular, the compressibility moduli calculated for simulations E1 and E2 with, respectively, the Berendsen and Parrinello–Rahman barostats are not statistically different. The two-tailed student's  $t$ -test  $p$  value for a difference of 200 mN/m is indeed 0.08. The only compressibility that is significantly different from the mean of the reported values is that of run H ( $p = 0.045$ ).

**D. Dipole Potential and Dipole Moments.** Lipid bilayers possess an internal dipole potential between the hydrocarbon interior and the aqueous phase surrounding the headgroups. This potential results from an ordering of the water dipoles at the interface that overcompensates for the contribution of the lipid dipoles. The dipole potential across the DPPC bilayer was determined as follows. The simulation box was divided into slices of 0.1-Å thickness perpendicular to the bilayer normal, and the time-averaged charge density was computed in each slice. The dipole potential profile along the bilayer normal was estimated by integrating this charge distribution twice using Poisson's equation:

$$\psi(z) - \psi(0) = -\frac{1}{\epsilon_0} \int_0^z dz' \int_0^{z'} \rho(z'') dz''$$

$\psi(z)$  and  $\rho(z)$  are the time-averaged dipole potential and charge density as a function of  $z$ , respectively, and  $\epsilon_0$  is the vacuum permittivity. The origin of the  $z$  axis was fixed in the middle of the water layer, where the potential was chosen to be zero. The potential curves were evaluated for different simulations and are plotted in Figure 5. The magnitude and the overall shape of the potential profiles are similar to those reported in previous simulations.<sup>46,47</sup> A positive potential of several hundred millivolts with respect to the water region is found in the bilayer interior. In the first set of simulations, a potential difference of  $620 \pm 20$  mV is generated with PME (average value over runs D, E1–3),  $720 \pm 100$  mV is generated with a cutoff of 1.8 nm (runs A and B1), and  $830 \pm 50$  mV is generated with RF (run F). The most striking difference between the three groups of simulations is the shape of the potential in the aqueous phase

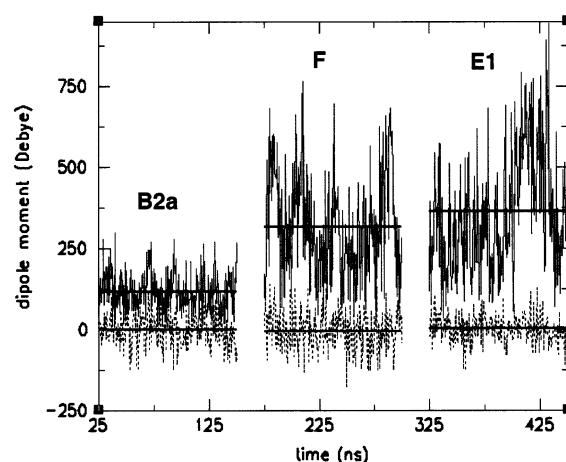


**Figure 6.** Lateral (solid-line curves) and perpendicular (dashed-line curves) box dipole moments as a function of time in simulations using either a Coulomb cutoff of 1.4 nm (B2a, left), RF (F, middle), or PME (E1, right). Averages are indicated by horizontal lines. The lateral dipole moment was calculated as  $(\mu_x^2 + \mu_y^2)^{1/2}$ ,  $\mu_x$  and  $\mu_y$  being the dipole moment components in the  $x$  and  $y$  directions, respectively.

(Figure 5). The potential is flat with PME and RF, whereas a potential drop within the water layer can be observed when a cutoff is applied. This can be explained by a significant long-range ordering of the water dipoles, a known artifact of truncation methods. Despite the long simulation time, the potential in the two halves of the bilayer is not completely symmetrical. This asymmetry is particularly pronounced in simulations using a cutoff, which might be another artifact of this technique.

The average overall dipole moments in the lateral ( $x$ ,  $y$ ) and perpendicular ( $z$ ) directions in the box and their fluctuations are shown in Figure 6 for straight cutoff (1.4 nm, run B2a), reaction field (F), and PME (E1) runs. The area per lipid in these three runs is comparable, and the differences in dipole moments should therefore be indicative of the effects of the electrostatics methods. The most striking feature observed in Figure 6 is the difference in the lateral dipole moment between straight cutoff and RF or PME. Both the average lateral dipole moment and its fluctuations are much smaller in the straight cutoff method. The difference between RF and PME is not very large. The average values of and fluctuations in the dipole moments appear to be somewhat larger in the PME approach. The magnitude of the lateral dipole moment found in the RF and PME simulations represents about 10% of the maximum possible for perfect alignment of the P–N dipoles. The distribution of the lateral dipole moment vector orientation is found to be random; the direction of the vector changes in time with a correlation time of about 10 ns for the straight cutoff simulations and about 40 ns for the RF and PME simulations.

**E. Diffusion Coefficients.** To determine whether dynamic properties of the bilayer are sensitive to the different simulation conditions, we compared the lateral diffusion coefficients of the DPPC molecules within the membrane plane. The lateral diffusion coefficient  $D_{\text{lat}}$  can be obtained from the slope of the lateral mean-square displacement (MSD) versus time:

$$D_{\text{lat}} = \lim_{t \rightarrow \infty} \frac{1}{4} \frac{d}{dt} \langle [r(t + t_0) - r(t_0)]^2 \rangle_{t_0}$$

The mean-square displacements were calculated for the center of mass (COM) of each DPPC molecule and averaged over time and over all of the lipid molecules.  $r$  represents the COM positions. To improve the statistics, the time origin  $t_0$  was shifted



**TABLE 3: Lateral Diffusion Coefficients**

label	$D_{\text{lat}} \pm \text{SE} (10^{-8} \text{ cm}^2/\text{s})$	
	uncorrected	corrected
A	350 $\pm$ 150	3.4 $\pm$ 0.4
B1	150 $\pm$ 50	8.4 $\pm$ 1.3
D	30 $\pm$ 3	12.0 $\pm$ 0.4
E1	40 $\pm$ 15	8.8 $\pm$ 0.5
E2	35 $\pm$ 5	8.2 $\pm$ 0.6
E3	15 $\pm$ 5	6.7 $\pm$ 0.7
F	150 $\pm$ 50	9.9 $\pm$ 0.7

every 25 ps. Before calculating mean-square displacements, a correction was introduced into the lipid coordinates. Although the center of mass of the whole system is reset after each step, both lipid layers can acquire some drift velocity and develop an opposite COM motion while the total COM motion for the system is still zero. The random relative motions of the two layers<sup>7</sup> give rise to an apparent supradiffusivity that is purely artificial and needs to be removed. For this reason, the DPPC coordinates were corrected by subtracting these monolayer COM motions. The uncorrected and corrected lateral diffusion coefficients were calculated over 62.5 ns, using data between 25 and 150 ns, and are given in Table 3. The corrected values for the diffusion coefficients are on the order of  $10 \times 10^{-8} \text{ cm}^2/\text{s}$  and are in good agreement with the coefficient of  $12 \times 10^{-8} \text{ cm}^2/\text{s}$  reported by Lindahl and Edholm<sup>7</sup> in a 100-ns DPPC simulation. Experimentally, Sheats and McConnell,<sup>48</sup> using a spin-label technique, measured a lateral diffusion coefficient ranging from  $9.9 \times 10^{-8}$  to  $12 \times 10^{-8} \text{ cm}^2/\text{s}$  in planar DPPC multilayers at about 48 °C. Kuo and Wade<sup>49</sup> determined the lateral diffusion coefficient of DPPC in multilayers by pulsed NMR at various temperatures and hydration levels. Interpolating their data at 323 K for 40 wt % water results in a coefficient of about  $9.5 \times 10^{-8} \text{ cm}^2/\text{s}$ . Orådd and co-workers,<sup>50</sup> also using pulsed NMR, found a lateral diffusion coefficient of about  $28 \times 10^{-8} \text{ cm}^2/\text{s}$  for DMPC at 323 K using an Arrhenius temperature dependence with an activation energy of 49 kJ/mol. Pace and Chan<sup>51</sup> predicted a coefficient of about  $15 \times 10^{-8} \text{ cm}^2/\text{s}$  from a jump-diffusion model for two-chain lipids at 323 K for a probability of jump success of 50%. Correlation between the area per lipid and the lateral diffusion coefficient is intuitively expected because larger areas would lead to an increased mobility of the lipid molecules and thus to higher diffusion coefficients. Although the diffusion coefficients obtained with PME or RF tend to be slightly larger than those obtained with a Coulomb cutoff (D vs A, E1 vs B1, or F vs B1), the observed differences are rather small and statistically insignificant. A truly diffusive regime is reached only at simulation times longer than 20 ns on average. In simulation A, a long-time diffusive behavior could not be observed.

#### IV. Discussion

A number of important conclusions can be drawn on the basis of the simulations in this paper. Although the simulations considered only one type of lipid and two similar force fields, we expect the effects we observe to be more generally valid.

**A. Equilibration Times on the Order of 10–20 ns Required for Phospholipid Simulations.** Clearly, long simulations are required to calculate basic equilibrium properties such as the area per lipid accurately. In the present simulations of the DPPC bilayer, the equilibration of the area per lipid requires on average 5 to 10 ns and even up to 25 ns in some cases. The slow convergence that is observed demonstrates that the generation of sufficient equilibrium sampling cannot definitely be obtained in simulations covering only a couple of nanosec-

onds. As previously found by Lindahl and Edholm<sup>6</sup> and Marrink and Mark,<sup>8</sup> large fluctuations of the membrane area with long correlation times (up to 10 ns) occur. These large area fluctuations can be attributed to the contribution from a hierarchy of motions, including the isomerization, rotation, and diffusion of individual lipids, as well as collective motions of the bilayer itself such as the appearance of undulations. Owing to this slow process of area fluctuations, simulations of multiple tens of nanoseconds are needed to trust the calculated average areas.

#### B. Area: Poor Judge of Methodology or Force Field.

Reproducing experimental values for the lipid area with care is particularly important because a large number of both structural and dynamic quantities are strongly connected to the area. Naturally, larger areas allow more disorder in the lipid tails, leading to an enhanced gauche population and decreased order parameters. The only exception seems to be the area compressibility, for which we do not observe a clear correlation with area.

Comparing the areas per lipid that we obtain for our DPPC systems using different methodological approaches (Table 2), it appears that almost any area per lipid can be reproduced. Areas as small as  $0.5 \text{ nm}^2$  or as large as  $0.7 \text{ nm}^2$  can be obtained with similar force fields. In contrast to the area, the volume per lipid does not appear to be very sensitive to methodological changes. For the area, the exact balance of forces between the headgroups and between the tails is crucial. The important question now is, Can we, on the basis of the obtained areas, judge the quality of the different algorithms and parameters? Clearly, the simulations corresponding to the extreme values for the area are wrong in the sense that they do not properly model a DPPC membrane, but DPPC bilayers with an area per lipid in the range  $0.62\text{--}0.66 \text{ nm}^2$ , within a few percent of the experimental value of  $0.63\text{--}0.64 \text{ nm}^2$ , are very similar in their properties. Interestingly, areas per lipid in this range can be obtained using significantly different methods. Whether using cutoffs, shift functions, RF, or PME, a reasonable area can be obtained. Therefore, the area per lipid is not a good measure of the quality of the force field or of methodology; the right combination of force field and methodology can always reproduce the proper area. As stated above, once the area is correct, most of the other properties appear to be reasonable, and this is why the large number of DPPC simulations available in the literature, using very different force fields and simulation methodologies, results in bilayers with very similar properties.

**C. Effect of Long-Range Interactions.** In the series of simulations performed, the area proved to be very sensitive to the details of the simulation and especially to the treatment of long-range electrostatic interactions. The observed effects can be explained by examining the properties of the electrostatics methods in conjunction with a simple model of a phospholipid bilayer. In a simple picture, the phospholipid bilayer system may be viewed as two constrained dipole layers with the zwitterionic headgroups as the basic dipoles constituting the layers. The lipid dipoles in a layer will generally be aligned roughly parallel to each other and to the bilayer normal because of the shape of the lipid molecule and headgroup hydration, thereby having a direct repulsive Coulomb interaction with each other. The dipole–dipole repulsion can be relieved by tilting the dipoles with respect to each other. Dipoles ideally adopt head–tail arrangements or align antiparallel to each other. In a bilayer, tilting the lipid headgroups is possible to a limited extent in the lateral directions. Once tilted in the lateral directions, the headgroups have more freedom to adopt favorable orientations. There are various energetic costs for this tilting. First,



tilting the headgroup requires a larger projected area of the lipid. The cost for this is the loss of attractive interactions in the tail region. Second, tilting the headgroup at the same area per lipid will reduce the hydration of the headgroup because a tilted headgroup is less exposed to water. This can be remedied by pulling the lipid out of the bilayer somewhat, which will again be at the cost of attractive interactions in the tail region. Third, condensing the headgroups into the plane of the membrane results in a loss of entropy.

In straight cutoff techniques, only short-range interactions are minimized. Tilting of the headgroup is seen to a limited extent and is reflected in a relatively small lateral dipole moment of the simulation box (Figure 6). In contrast, both PME and RF show a large lateral box dipole moment due to strong tilting of the headgroup dipoles in the lateral directions. Tilting of headgroups into the bilayer plane is the cheapest way of building up dipole moments and is rewarded energetically in both Ewald and RF methods. Ewald methods may thus induce artifacts by building up large simulation cell dipoles that are being replicated into infinity and interact favorably with each other. The reaction field model stabilizes local dipole moments. This results in a lateral expansion of the bilayers compared to straight cutoff methods (compare A and B1–3 to F, and I1–3 to K1–3). The difference between RF and PME for the area per lipid depends on the balance of forces within the bilayer. For the first force field, RF (cutoff 1.8 nm) and PME give very similar areas (compare F and E), whereas for the second force field the area with RF is larger than with PME (compare K and J). The RF approach seems to converge to the PME result if the cutoff radius is increased (compare runs K1–3 to J), which is expected because the “local” dipole moment within the cutoff sphere approaches the box dipole moment with increasing cutoff. Unfortunately, with large cutoffs, the RF method becomes impractical because of the loss of computational speed.

Another possible artifact for bilayer systems in Ewald methods is the arrangement of dipoles parallel to an axis at half the axis size. In this particular arrangement, the forces between parallel dipoles are zero, introducing strong spatial correlation into the system.<sup>52</sup> If the system is small enough, then this could be a considerable driving force. The tendency of the unit cell to become rather asymmetric in the smaller system (runs D, E1,2, and H) may find its origin in the fact that two charges do not exert a force on each other at a distance  $L/2$ , where  $L$  is the dimension of the unit cell. However, as the dimension of the unit cell exceeds the mean headgroup–headgroup distance many times, the long-range ordering artifact is counteracted by stronger fluctuations induced by the short-range interactions. The PME run done on the larger system (J) did not show a strong tendency toward an asymmetric unit cell. However, for pure bilayer systems that are not too small, Ewald techniques appear to be more appropriate than straight cutoff methods to the simulation of fluid-phase bilayers, but one should realize that in mixed systems (i.e., bilayers with drugs or proteins embedded or with water channels inside) standard 3D Ewald methods can create artificial order.<sup>25</sup>

The effects on the area of the bilayer observed with increased cutoff distance with the straight cutoff technique are reminiscent of the contraction of dipolar systems on increasing the electrostatic cutoff described for pure liquids.<sup>12,18</sup> The contraction is explained by the build up of favorable interactions just inside the cutoff sphere, reducing the outward pressure of the system. The nonneutrality of the charge groups gives rise to the creation of artificial charges, which causes an even stronger lateral long-range attraction in the bilayer, analogous to the effects observed

in ionic systems.<sup>13,18</sup> Increasing the cutoff only makes things worse. (Compare runs B1–3 and runs I1–3.) The effect increases with increasing cutoff distance because the number of these favorable interactions grows faster (scaling with  $r^2$ ) than the strength of the interaction diminishes (which goes as  $1/r$  because of the nonneutral charge groups).

As an alternative method, one could use a shift function with or without a reaction field correction to the energy. It avoids the artifacts arising from cutting through dipoles as in straight cutoff methods, and it also avoids dipole correlations across the simulation cell possible with Ewald methods. The RF method has already been discussed. The GROMACS shift function appears to be intermediate between straight cutoff and RF. On one hand, it does not suffer from the dipole–dipole correlation artifact associated with straight cutoff, but on the other hand, it avoids a large lateral dipole moment as seen with RF. If computational speed is important and one wants to avoid the artifacts from cutting dipoles, the use of shift functions is appealing, although a larger dependence on cutoff distance was observed with the shift function as compared to the RF approach and instabilities in the simulations were registered as the cutoff distance was increased.

Apart from the long-range electrostatic interactions, the long-range dispersion interactions can also have a significant effect on the membrane properties through the modulation of the system density. Including a long-range dispersion correction for the Lennard-Jones interactions (run B2b) produces a slight decrease in the area but a net decrease in the volume per lipid, resulting in a clear contraction of the membrane. The LJ interactions also account for small but significant changes in area observed upon increasing the number of charge groups with PME, as can be seen from the comparison of runs D and E1.

**D. Effect of Pressure Coupling and Time Step.** The type of pressure-coupling scheme appears to have no significant effect on the equilibrium properties of the bilayer (compare E1 and E2). Although the Parrinello–Rahman method is to be preferred on theoretical grounds (in contrast to the Berendsen method, it generates a well defined ensemble), the Berendsen scheme is more practical because it damps large oscillations in box dimensions that may occur, especially during the equilibration stage. Caution is needed when coupling anisotropically. If one of the lateral dimensions becomes too small, periodic ordering effects appear, especially when using PME. For larger systems, the anisotropy is not worrisome because it does not seem to influence any of the system properties. Finally, the current constraining algorithms allow a time step of 5 fs, which can be safely used in phosphatidylcholine bilayer simulations (compare B1 and C).

## V. Conclusions

The series of simulations presented in this paper show that 10 to 20 ns of equilibration time are required for MD studies of phospholipid bilayers. The area per lipid is observed to be very sensitive to the simulation conditions, especially to the treatment of long-range electrostatics. As long as the area remains within the experimental range, reasonable lipid properties are observed. With the right combination of methodology and force field, lipid bilayers with areas close to the experimentally determined one can be obtained with any approach to treating the long-range electrostatics. Benefits and artifacts of each method can be pointed out, demonstrating that none of these methods is perfect for the simulation of interfacial systems. Straight cutoff methods, however, most clearly show some unwanted ordering effects and should be avoided in pure bilayer

simulations. Instead of straight cutoff methods, shift functions can be applied: artificial correlation effects are removed, and computational speed is maintained. In the present simulations of DPPC bilayer systems, PME and RF approaches seem to be the most reasonable options, leading to stable runs and alleviating severe artifacts. It is further shown that time steps in combination with proper constraining algorithms and a united-atom model can be taken up to 5 fs. Details of the pressure scaling method appear to be unimportant to the observed bilayer properties.

**Acknowledgment.** A.H.V. acknowledges support from MSC<sup>plus</sup>. D.P.T. is a Scholar of the Alberta Heritage Foundation for Medical Research. D.P.T. acknowledges support from the NSERC. S.-J.M. is supported by the Royal Dutch Academy of Science (KNAW).

## References and Notes

- (1) Blume, A. Dynamic Properties. In *Phospholipids Handbook*; Cevc, G., Ed.; Marcel Dekker: New York, 1993; pp 455–509.
- (2) Essmann, U.; Berkowitz, M. L. *Biophys. J.* **1999**, *76*, 2081.
- (3) Feller, S. E.; Huster, D.; Gawrisch, K. *J. Am. Chem. Soc.* **1999**, *121*, 8963.
- (4) Moore, P. B.; Lopez, C. F.; Klein, M. L. *Biophys. J.* **2001**, *81*, 2484.
- (5) Pastor, R. W.; Venable, R. M.; Feller, S. E. *Acc. Chem. Res.* **2002**, *35*, 438.
- (6) Lindahl, E.; Edholm, O. *Biophys. J.* **2000**, *79*, 426.
- (7) Lindahl, E.; Edholm, O. *J. Chem. Phys.* **2001**, *115*, 4938.
- (8) Marrink, S. J.; Mark, A. E. *J. Phys. Chem. B* **2001**, *105*, 6122.
- (9) Darden, T.; York, D.; Pedersen, L. *J. Chem. Phys.* **1993**, *98*, 10089.
- (10) Essmann, U.; Perera, L.; Berkowitz, M. L.; Darden, T.; Lee, H.; Pedersen, L. G. *J. Chem. Phys.* **1995**, *103*, 8577.
- (11) Norberg, J.; Nilsson, L. *Biophys. J.* **2000**, *79*, 1537.
- (12) Hess, B. *J. Chem. Phys.* **2002**, *116*, 209.
- (13) Tironi, I. G.; Sperb, R.; Smith, P. E.; van Gunsteren, W. F. *J. Chem. Phys.* **1995**, *102*, 5451.
- (14) Feller, S. E.; Pastor, R. W.; Rojnuckarin, A.; Bogusz, S.; Brooks, B. R. *J. Phys. Chem.* **1996**, *100*, 17011.
- (15) Hünenberger, P. H.; van Gunsteren, W. F. *J. Chem. Phys.* **1998**, *108*, 6117.
- (16) Mark, P.; Nilsson, L. *J. Comput. Chem.* **2002**, *23*, 1211.
- (17) Alper, H. E.; Bassolino, D.; Stouch, T. R. *J. Chem. Phys.* **1993**, *98*, 9798.
- (18) Brooks, C. L., III; Pettitt, B. M.; Karplus, M. *J. Chem. Phys.* **1985**, *83*, 5897.
- (19) Smith, P. E.; Pettitt, B. M. *J. Chem. Phys.* **1996**, *105*, 4289.
- (20) Smith, P. E.; Blatt, H. D.; Pettitt, B. M. *J. Phys. Chem. B* **1997**, *101*, 3886.
- (21) Weber, W.; Hünenberger, P. H.; McCammon, J. A. *J. Phys. Chem. B* **2000**, *104*, 3668.
- (22) Venable, R. M.; Brooks, B. R.; Pastor, R. W. *J. Chem. Phys.* **2000**, *112*, 4822.
- (23) Yeh, I.-C.; Berkowitz, M. L. *J. Chem. Phys.* **1999**, *111*, 3155.
- (24) De Joannis, J.; Arnold, A.; Holm, C. *J. Chem. Phys.* **2002**, *117*, 2503.
- (25) Bostick, D.; Berkowitz, M. L. *Biophys. J.* **2003**, *85*, 97.
- (26) Tieleman, D. P.; Hess, B.; Sansom, M. S. P. *Biophys. J.* **2002**, *83*, 2393.
- (27) Tieleman, D. P.; Berendsen, H. J. C. *J. Chem. Phys.* **1996**, *105*, 4871.
- (28) Feller, S. E.; Pastor, R. W. *J. Chem. Phys.* **1999**, *111*, 1281.
- (29) Nagle, J. F.; Zhang, R.; Tristram-Nagle, S.; Sun, W.; Petrache, H. I.; Suter, R. M. *Biophys. J.* **1996**, *70*, 1419.
- (30) Berger, O.; Edholm, O.; Jähnig, F. *Biophys. J.* **1997**, *72*, 2002.
- (31) *TRC Thermodynamic Tables: Hydrocarbons*; Texas A&M University System: College Station, TX, 1986.
- (32) Schuler, L. D.; Daura, X.; van Gunsteren, W. F. *J. Comput. Chem.* **2001**, *22*, 1205.
- (33) Chiu, S.-W.; Clark, M.; Balaji, V.; Subramaniam, S.; Scott, H. L.; Jakobsson, E. *Biophys. J.* **1995**, *69*, 1230.
- (34) Berendsen, H. J. C.; Postma, J. P. M.; van Gunsteren, W. F.; Hermans, J. Interaction Models for Water in Relation to Protein Hydration. In *Intermolecular Forces*; Pullman, B., Ed.; Reidel: Dordrecht, The Netherlands, 1981; pp 331–342.
- (35) Smith, P. E.; van Gunsteren, W. F. *J. Chem. Phys.* **1994**, *100*, 3169.
- (36) Van der Spoel, D.; van Buuren, A. R.; Apol, E.; Meulenhoff, P. J.; Tieleman, D. P.; Sijbers, A. L. T. M.; Hess, B.; Feenstra, K. A.; Lindahl, E.; van Drunen, R.; Berendsen, H. J. C. *Gromacs User Manual*, version 3.0; Nijenborgh 4, 9747 AG Groningen: The Netherlands, 2001. The form of the modified Coulomb potential function or shift function used in the present work is the following:  $U(r) = 1/r - 5/(3R_C) + 5r^3/(3R_C^4) - r^4/(R_C^5)$ , where  $R_C$  is the Coulomb cutoff.
- (37) Zhang, Y. H.; Feller, S. E.; Brooks, B. R.; Pastor, R. W. *J. Chem. Phys.* **1995**, *103*, 10252.
- (38) Berendsen, H. J. C.; Postma, J. P. M.; van Gunsteren, W. F.; DiNola, A.; Haak, J. R. *J. Chem. Phys.* **1984**, *81*, 3684.
- (39) Parrinello, M.; Rahman, A. *J. Appl. Phys.* **1981**, *52*, 7182.
- (40) Berendsen, H. J. C.; van der Spoel, D.; van Drunen, R. *Comput. Phys. Commun.* **1995**, *91*, 43.
- (41) Hess, B.; Bekker, H.; Berendsen, H. J. C.; Fraaije, J. G. E. M. *J. Comput. Chem.* **1997**, *18*, 1463.
- (42) Miyamoto, S.; Kollman, P. A. *J. Comput. Chem.* **1992**, *13*, 952.
- (43) Feenstra, K. A.; Hess, B.; Berendsen, H. J. C. *J. Comput. Chem.* **1999**, *20*, 786.
- (44) Petrache, H. I.; Dodd, S. W.; Brown, M. F. *Biophys. J.* **2000**, *79*, 3172.
- (45) Nagle, J. F.; Tristram-Nagle, S. *Biochim. Biophys. Acta* **2000**, *1469*, 159.
- (46) Smdyrev, A. M.; Berkowitz, M. L. *J. Comput. Chem.* **1999**, *20*, 531.
- (47) Smdyrev, A. M.; Berkowitz, M. L. *Biophys. J.* **2000**, *78*, 1672.
- (48) Sheats, J. R.; McConnell, H. M. *Proc. Natl. Acad. Sci. U.S.A.* **1978**, *75*, 4661.
- (49) Kuo, A.-L.; Wade, C. G. *Biochemistry* **1979**, *18*, 2300.
- (50) Orädd, G.; Lindblom, G.; Westerman, P. W. *Biophys. J.* **2002**, *83*, 2702.
- (51) Pace, R. J.; Chan, S. I. *J. Chem. Phys.* **1982**, *76*, 4241.
- (52) Hünenberger, P. H. In *Simulation and Theory of Electrostatic Interactions in Solution*; Pratt, L. R., Hummer G., Eds.; AIP Conference Proceedings, 1999.